BINARY STARS and TYPE Ia SUPERNOVAE

18.1 Close Binary Star Systems

It is thought that about half of the stars in the sky are in multiple systems, consisting of two or more stars in orbit about the common centre of mass. In most of these systems, the stars are sufficiently far apart that they have little impact on one another, and evolve independently of one another, except for the fact that they are bound to each other by gravity.

In this lecture we will consider close binary systems, where the distance separating the stars is comparable to their size. In this situation, the outer layers of the stars can become deformed by the gravity of the companion. Under the right circumstances, matter can be transferred from one star to the other with far-reaching consequences for the evolution of the two stars. We begin by considering how gravity operates in a close binary system.

18.1.1 Lagrangian Points and Equipotential Surfaces

Consider two stars in circular orbits about their common centre of mass in the x–y plane with angular velocity $\omega = v_1/r_1 = v_2/r_2$, where v is the orbital speed and r the distance from the centre of mass of the system. When considering such a system, it is convenient to work in a corotating coordinate system with the centre of mass at the origin (Figure 18.1), and the mutual gravitational attraction between the two stars balanced by the outward push of a centrifugal force.

In this frame of reference, the centrifugal force vector on a mass m at a distance r from the origin is:

$$\mathbf{F}_c = m\omega^2 r\,\hat{\mathbf{r}} \tag{18.1}$$

in the outward radial direction. When considering the potential energy of the system in a corotating coordinate system, we add to the gravitational

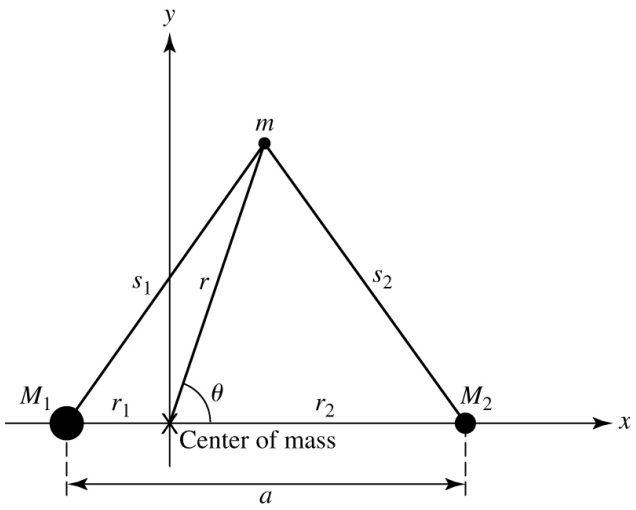

Figure 18.1: Corotating coordinates for a binary star system. Note that $a = r_1 + r_2$ and $M_1 r_1 = M_2 r_2$. In the examples considered in the text, $M_1 = 0.85 M_\odot$, $M_2 = 0.17 M_\odot$ and $a = 0.718 R_\odot$.

potential energy:

$$U_g = -G\frac{Mm}{r} \tag{18.2}$$

a *"centrifugal potential energy"*

$$U_c = -\frac{1}{2}m\omega^2 r^2 \tag{18.3}$$

obtained by integrating eq. 18.1 with the boundary condition $U_c = 0$ at $r = 0$. Including the centrifugal term, the effective potential energy for a small test mass m located in the plane of the orbit is:

$$U = -G\left(\frac{M_1 m}{s_1} + \frac{M_2 m}{s_2}\right) - \frac{1}{2}m\omega^2 r^2 \,. \tag{18.4}$$

Dividing by m, we obtain the effective potential energy per unit mass, or the **effective gravitational potential**, Φ:

$$\Phi = -G\left(\frac{M_1}{s_1} + \frac{M_2}{s_2}\right) - \frac{1}{2}\omega^2 r^2 \,. \tag{18.5}$$

Returning to Figure 18.1, we have (from the law of cosines):

$$s_1^2 = r_1^2 + r^2 + 2r_1 r\cos\theta \tag{18.6}$$

$$s_2^2 = r_2^2 + r^2 - 2r_2 r\cos\theta \,. \tag{18.7}$$

The angular frequency of the orbit, ω, is given by Kepler's third law:

$$\omega^2 = \left(\frac{2\pi}{P}\right)^2 = \frac{G\left(M_1 + M_2\right)}{a^3} \,. \tag{18.8}$$

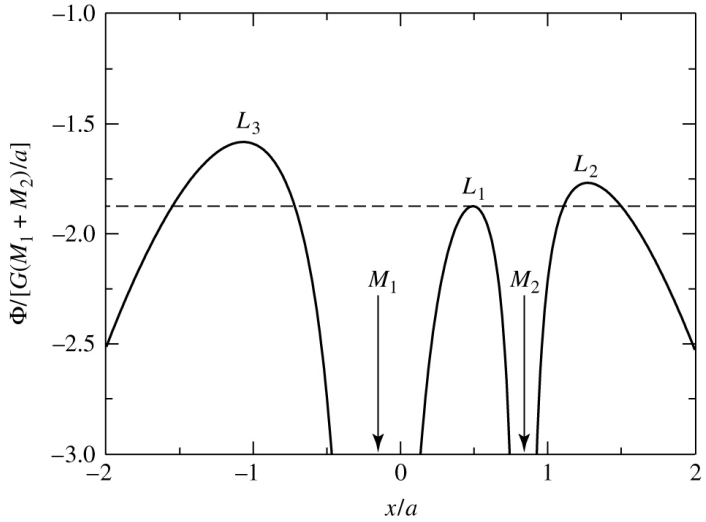

Figure 18.2: The effective gravitational potential Φ along the x-axis for two stars with masses $M_1 = 0.85M_\odot$ and $M_2 = 0.17M_\odot$. The stars are separated by a distance $a = 0.718R_\odot$ (see Figure 18.1). The dashed line is the value of Φ at the inner Lagrangian point. If the total energy per unit mass of a particle exceeds this value of Φ, it can flow through the inner Lagrangian point between the two stars.

The last four equations can be used to evaluate the effective gravitational potential Φ at every point in the orbital plane of a binary star system. For example, Figure 18.2 shows the value of Φ along the x-axis. The significance of this graph becomes clear when we consider the x-component of the force on a small test mass m, initially at rest on the x-axis:

$$F_x = -\frac{dU}{dx} = -m\frac{d\Phi}{dx} \tag{18.9}$$

At the values of x/a labelled L_n, $d\Phi/dx = 0$, and therefore there is no net force on the test mass: the gravitational pull exerted on m by M_1 and M_2 is just balanced by the centrifugal force of the rotating reference frame. These are the **Lagrangian points**. In a non-rotating reference frame, the Lagrangian points mark positions where the combined gravitational pull of the two masses on a test mass provides precisely the centripetal force required for the test mass to rotate with them. Thus, at these points a test mass maintains its position relative to the two stars. These equilibrium points are clearly unstable because they are local maxima of Φ: perturb the test mass slowly and it will accelerate down the potential.

As we shall see presently, the *inner Lagrangian point*, L_1, is central to the evolution of close binary systems. Approximate expressions for the

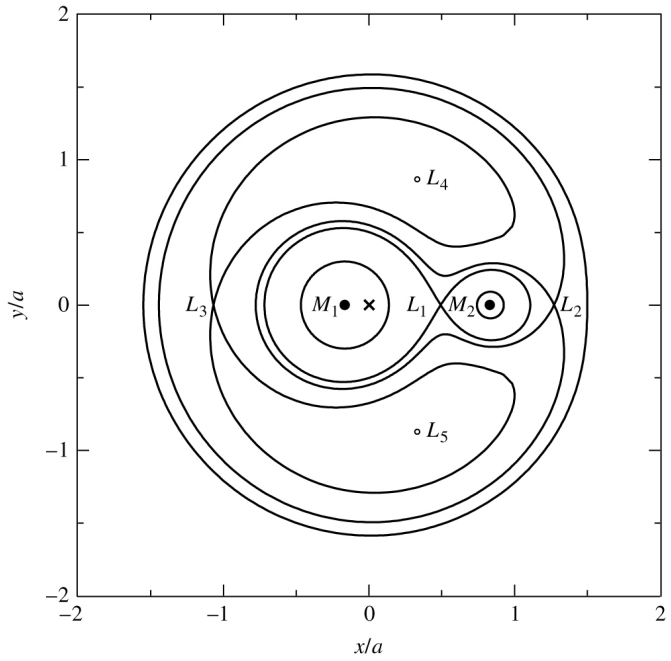

Figure 18.3: Intersections of equipotential surfaces with the plane of the orbit of a close binary system with masses $M_1 = 0.85M_\odot$, $M_2 = 0.17M_\odot$ and separation $a = 0.718R_\odot$ (see Figure 18.1). The centre of mass of the system is indicated with the '×' symbol.

distances from L_1 to M_1 and M_2, denoted ℓ_1^1 and ℓ_1^2 respectively, are:

$$\ell_1^1 = a\left[0.500 - 0.227\log_{10}\left(\frac{M_2}{M_1}\right)\right] \tag{18.10}$$

$$\ell_1^2 = a\left[0.500 + 0.227\log_{10}\left(\frac{M_2}{M_1}\right)\right] \tag{18.11}$$

Points in space that share the same value of Φ define an equipotential surface. Figure 18.3 shows equipotential contours on the plane of the orbit for the binary system illustrated in Figure 18.1. Very close to each of the two masses, the equipotential surfaces are nearly spherical and centred on each mass. However, further away, the combined gravitational influence of M_1 and M_2 distorts the equipotential surfaces into teardrop shapes until they touch at the inner Lagrangian point. At greater distances, the equipotential surfaces assume a 'dumbbell' shape surrounding both masses.

These equipotential surfaces are *level surfaces* for binary stars. In such systems, as a star evolves it will expand to fill successively larger equipotential surfaces. This is easy to see when we consider that the effective gravity at each point is always perpendicular to the equipotential surface at that point. As there is no gravity parallel to an equipotential surface, a pressure difference in that direction cannot be maintained. It follows that

the density must also be the same along each equipotential surface in order to have a constant pressure there.

18.1.2 Classes of Binary Stars

Binary stars are classified on the basis of which equipotential surfaces are filled. In detached binaries, the distance separating the two stars is much greater than their radii. The stellar surfaces are close to spherical (see Figure 18.4) and the two stars evolve nearly independently of each other. These are the systems which, as we discussed in Lecture 4, provide us with measures of stellar masses from observations of their orbital periods.

However, if one of the two stars in the course of its evolution expands to fill its equipotential surface up to the inner Lagrangian point L_1, its atmospheric gases can escape and be drawn towards its companion. The teardrop-shaped regions of space bounded by this particular equipotential surface are called *Roche lobes*; when one of the stars in a binary system has expanded beyond its Roche lobe, mass transfer to its companion can take place. Such a system is called a semidetached binary (middle panel of

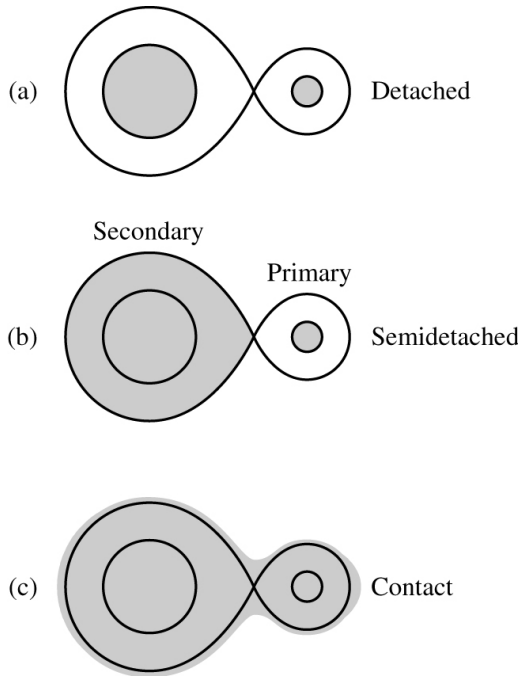

Figure 18.4: Different classes of binary systems. In semidetached binaries (b), the secondary has expanded to fill its Roche lobe. In contact binaries (c), the two stars share a common atmosphere.

Figure 18.4). The star that has filled its Roche lobe and is losing mass is usually referred to as the *secondary star* in the system with mass M_2, and its accreting companion is the *primary star* with mass M_1. Note that the primary star can be either more or less massive than the secondary star.

It may also be the case that *both* stars expand to (over)fill their Roche lobes. In this case, the two stars share a common atmosphere bounded by a dumbbell-shaped equipotential surface, such as the one passing through the Lagrangian point L_2. Such systems are referred to as *contact binaries* (Figure 18.4).

The three cases illustrated in Figure 18.4, together with a range of stellar types, give rise to a rich nomenclature of different classes of interacting binary systems. Here we mention just two.

Cataclysmic Variables consist of a white dwarf primary and an M-type secondary filling its Roche lobe. They have short periods and irregularly increase in brightness by a large factor, then drop back to a quiescent state. Much attention is focused on CVs because they provide valuable information on final stages of stellar evolution and on accretion disks (see below).

X-ray Binaries have a neutron star or black hole component. The X-rays are generated by the accretion of gas onto the degenerate star from a non-degenerate companion. Observations of neutron star X-ray binaries complement the information on their physical properties (such as masses, radii, rotation and magnetic fields) obtained from pulsar studies.

Cygnus X-1 was the first X-ray source widely accepted to be a black hole candidate. Its mass is estimated to be $8.7 M_\odot$, and it has been shown to be too compact to be any kind of object other than a black hole. Cygnus X-1 belongs to a high-mass X-ray binary system that includes the blue supergiant HDE 226868; the separation of the two objects is only ~ 0.2 AU. A stellar wind from the blue supergiant provides material for an accretion disk around the X-ray source. Matter in the inner disk is heated to millions of degrees, generating the observed X-rays. A pair of jets perpendicular to the disk are carrying part of the infalling material away into interstellar space.

18.1.3 Accretion Disks

The orbital motion of a semidetached binary can prevent the mass that escapes from the swollen secondary star from falling directly onto the primary. Instead, the mass stream goes into orbit around the primary to form a thin accretion disk of hot gas in the orbital plane, as shown in Figure 18.5.

A key component of accretion disk physics is *viscosity*, an internal friction that converts kinetic energy of bulk mass motion into random thermal motion. If matter is to fall inwards it must lose not only gravitational energy but also angular momentum. Since the total angular momentum of the disc is conserved, the angular momentum loss of the mass falling into the centre has to be compensated by an angular momentum gain of the mass far from the centre. In other words, angular momentum should be *transported* outwards for matter to accrete. Turbulence enhanced viscosity is the mechanism thought to be responsible for such angular momentum redistribution, although the origin of the turbulence itself is not fully understood. It is likely that magnetic fields play a role.

Accretion disks continue to be an active area of astrophysical research, both theoretical and observational. One of the reasons for the continued interest in this phenomenon is the ubiquity of accretion disks, from protostars and protoplanetary disks to binary stars, gamma-ray bursts, and active galactic nuclei.

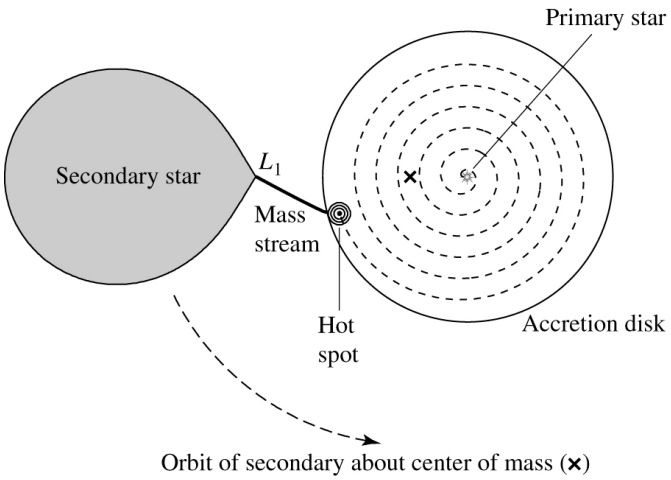

Figure 18.5: A semidetached binary showing the accretion disk around the primary star and the hot spot where the mass streaming through the inner Lagrangian point impacts the disk.

18.1.4 The Effects of Mass Transfer

The life history of a close binary system is quite complicated, with many possible variations depending on the initial masses and separations of the two stars involved. As mass is transferred from one star to the other, the mass ratio M_2/M_1 will change. The resulting redistribution of angular momentum affects the orbital period of the system, $P = \sqrt{2\pi}/\omega$, as well as the separation of the two stars, a. The extent of the Roche lobes, given by eqs. 18.10 and 18.11, depends on both a and M_2/M_1, so it too will vary accordingly.

The effects of mass transfer can be illustrated with a simple analytical treatment that considers the total angular momentum of the binary system. Assuming circular orbits, the orbital angular momentum of the binary system is given by the expression:

$$L = \mu\sqrt{GMa} \tag{18.12}$$

where μ is the reduced mass:

$$\mu = \frac{M_1 M_2}{M_1 + M_2} \tag{18.13}$$

and $M = M_1 + M_2$ is the total mass of the two stars.

Assuming to a first approximation that no mass or angular momentum is removed from the system via stellar winds or gravitational radiation, both the total mass and the angular momentum of the system are conserved as mass is transferred between the two stars. That is, $dM/dt = 0$ and $dL/dt = 0$.

Taking the time derivative of the angular momentum, we have:

$$\begin{aligned} \frac{dL}{dt} &= \frac{d}{dt}\left(\mu\sqrt{GMa}\right) \\ 0 &= \sqrt{GM}\left(\frac{d\mu}{dt}\sqrt{a} + \frac{\mu}{2\sqrt{a}}\frac{da}{dt}\right) \\ \frac{1}{a}\frac{da}{dt} &= -\frac{2}{\mu}\frac{d\mu}{dt}\,. \end{aligned} \tag{18.14}$$

Differentiating (18.13), we have:

$$\frac{d\mu}{dt} = \frac{1}{M}\left(\dot{M}_1 M_2 + \dot{M}_2 M_1\right) \tag{18.15}$$

since $M = M_1 + M_2$ is constant. Furthermore, from the condition that $dM/dt = 0$, it follows that $\dot{M}_1 = -\dot{M}_2$, and therefore,

$$\frac{d\mu}{dt} = \frac{\dot{M}_1}{M}\left(M_2 - M_1\right) . \tag{18.16}$$

Substituting 18.16 into 18.14, we arrive at our result:

$$\frac{1}{a}\frac{da}{dt} = 2\dot{M}_1 \frac{M_1 - M_2}{M_1 M_2} \tag{18.17}$$

which describes how the binary separation a varies as a result of mass transfer from M_2 to M_1. Note that in the cases mentioned above, where the primary is a compact object, $M_1 < M_2$, so that da/dt is $-$ve: the stars get closer together.

The angular frequency ω of the orbit will also be affected, according to eq. 18.8. Since M_1+M_2 is constant, Kepler's third law states that $\omega \propto a^{-3/2}$, and:

$$\frac{1}{\omega}\frac{d\omega}{dt} = -\frac{3}{2}\frac{1}{a}\frac{da}{dt} . \tag{18.18}$$

As the orbit shrinks, the angular frequency increases.

18.2 Type Ia Supernovae

As we discussed in Lecture 14, there is a limit to the mass of a white dwarf that can be supported by electron degeneracy pressure. This limit, known as the Chandrasekhar limit, is estimated to be $1.44M_\odot$ in the absence of significance rotation.

In close binary systems, mass transfer between the two stars may cause a white dwarf to approach the Chandrasekhar mass, leading to a catastrophic stellar explosion which we witness as a Type Ia supernova (Lecture 16.3). However, the details of the mechanism(s) that trigger the explosion are still unclear and the subject of much ongoing research. One of the problems is to understand why, when the Chandrasekar limit is exceeded, the white dwarf does not 'just' collapse to form a neutron star.

18.2.1 Single Degenerate Scenario

The single degenerate scenario involves an evolving star transferring mass onto the surface of a white dwarf companion as in Figure 18.5. The current view among astronomers who model Type Ia supernova explosions is that in such systems the Chandrasekhar limit is never actually attained, so that collapse is never initiated. Instead, the increase in pressure and density due to the increasing mass of the white dwarf raises the temperature of the core and, as the white dwarf approaches to within $\sim 1\%$ of the Chadrasekhar limit, a period of convection ensues, lasting approximately 1,000 years. At some point in this simmering phase, carbon fusion is ignited. The details of the ignition are still unknown, including the location and number of points where the flame begins. Oxygen fusion is initiated shortly thereafter, but this fuel is not consumed as completely as carbon.

Once fusion has begun, the temperature of the white dwarf starts to rise. A main sequence star supported by thermal pressure would expand and cool in order to counterbalance an increase in thermal energy. However, as we have already discussed in previous lectures, degeneracy pressure is independent of temperature. Thus, the white dwarf is unable to regulate the burning process in the manner of normal stars, leading to a thermonuclear runaway. What happens next is also a matter of debate. It is unclear if the CO burning front occurs at subsonic speeds (normally referred to as a '*deflagration*' event), or if the front accelerates and steepens to become a supersonic burning front, known as a '*detonation*', or true explosion.

Regardless of the exact details of nuclear burning, it is generally accepted that a substantial fraction of the carbon and oxygen in the white dwarf is burned into heavier elements within a period of only a few seconds, raising the internal temperature to billions of degrees. The energy release from thermonuclear burning, $E \sim 1\text{–}2 \times 10^{51}$ erg, exceeds the binding energy of the star; the star explodes violently and releases a shock wave in which matter is typically ejected at speeds of $\sim 5\,000\text{–}20{,}000\,\mathrm{km\ s^{-1}}$. Whether or not the supernova remnant remains bound to its companion depends on the amount of mass ejected.

This scenario is similar to that of novae, in which a WD accretes matter more slowly and does not approach the Chandrasekhar limit. The infalling matter causes a H fusion surface explosion that does not disrupt the star.

18.2.2 Double Degenerate Models

As the name implies, double degenerate models involve two white dwarfs in a binary orbit. Such systems are known to exist and it is a seemingly inevitable consequence that the two stars will spiral together as the system loses energy and angular momentum by gravitational radiation. On the other hand, computer simulations suggest that, as the two stars get very close together, the lighter of the two white dwarfs is torn apart and forms a thick disk around the other. This leads to an off-centre carbon ignition, resulting in ultimate collapse to a neutron star, rather than complete disruption of the white dwarf as a supernova.

Both the single- and the double-degenerate models have their strengths and their weaknesses. Of course, both mechanisms may be at work in nature, but we still do not know which is the dominant one. Furthermore, fundamental questions remain as to how the accretion of matter leads to the explosion in each progenitor model.

18.2.3 Nucleosynthesis in Type Ia Supernovae

The spectra of Type Ia supernovae taken near maximum light show absorption lines of intermediate mass elements, primarily O, Mg, Si, S, and Ca. These elements are produced by the rapid fusion of C and O via the channels already considered in Lecture 7.4.4:

$$
\begin{aligned}
{}^{12}\mathrm{C} + {}^{12}\mathrm{C} &\rightarrow {}^{16}\mathrm{O} + 2\,{}^{4}\mathrm{He} \\
&\rightarrow {}^{20}\mathrm{Ne} + {}^{4}\mathrm{He} \\
&\rightarrow {}^{23}\mathrm{Na} + p^{+} \\
&\rightarrow {}^{23}\mathrm{Mg} + n \\
&\rightarrow {}^{24}\mathrm{Mg} + \gamma
\end{aligned}
\qquad\qquad
\begin{aligned}
{}^{16}\mathrm{O} + {}^{16}\mathrm{O} &\rightarrow {}^{24}\mathrm{Mg} + 2\,{}^{4}\mathrm{He} \\
&\rightarrow {}^{28}\mathrm{Si} + {}^{4}\mathrm{He} \\
&\rightarrow {}^{31}\mathrm{P} + p^{+} \\
&\rightarrow {}^{31}\mathrm{S} + n \\
&\rightarrow {}^{32}\mathrm{S} + \gamma
\end{aligned}
$$

At later epochs, the spectra become dominated by Fe and other heavy elements produced by explosive nucleosynthesis. Evidently, the outer ejecta show the products of C and O burning, while the inner, denser regions of the exploding star burn all the way to the Fe-group. The presence of high-velocity C and O in early-time spectra suggests that the explosion left behind some unburnt material, possibly in pockets.

The primary iron-peak element produced by the explosion is $^{56}_{28}$Ni, because the timescale of explosive nucleosynthesis is too short for β-decay to change the original proton to neutron ratio from Z/A = 1/2 of the fuel $^{28}_{14}$Si. $^{56}_{28}$Ni decays to $^{26}_{56}$Fe via the reactions:

$$^{56}_{28}\mathrm{Ni} \rightarrow ^{56}_{27}\mathrm{Co} + \mathrm{e}^{+} + \nu_e + \gamma \qquad (\tau_{1.2} = 6.1\,\mathrm{days})$$
$$^{56}_{27}\mathrm{Co} \rightarrow ^{56}_{26}\mathrm{Fe} + \mathrm{e}^{+} + \nu_e + \gamma \qquad (\tau_{1.2} = 77.7\,\mathrm{days})$$

powering the light curve of Type Ia supernovae which shows a two-step decline (see Figure 18.6). Analysis of the light curve indicates that, typically, the ejected mass of $^{56}_{28}$Ni is ~ 0.7–$1\,M_{\odot}$.

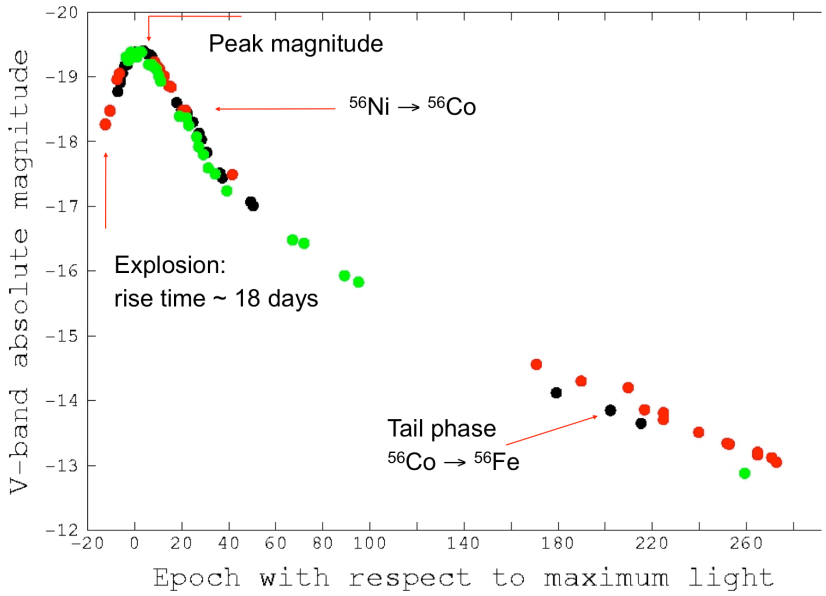

Figure 18.6: Typical light curve of a Type Ia supernova, constructed by combining the light curves of SN1990N, SN1996X and SN2002er.

Much effort has been devoted to computational modelling of nucleosynthesis in exploding CO white dwarfs, with a good degree of success in matching the temporal evolution of their spectra. SN Ia are thought to be the source of $\sim 2/3$ of the Fe which has accumulated in the interstellar medium up to the present-day. An origin in low and intermediate mass stars introduces a time-lag in the release of Fe compared to the prompt release of O and other alpha-capture elements from Type II supernovae which, as you will remember, have massive star progenitors. This fact has been much exploited by models that attempt to reconstruct the past history of star formation in galaxies from measurements of the relative abundances of different elements as a function of time.

18.2.4 SN 2011fe

Our ideas about the progenitors of Type Ia supernovae are largely driven by theoretical considerations based on circumstantial evidence, such as the lack of H and He lines in their spectra (few astrophysical objects lack these elements); their occurrence in galaxies of all types, rather than being associated exclusively with regions of star formation, as is the case for Type II SNe; and the consistency between the energy generated by burning a CO white dwarf and that associated with Type Ia SN events.

The reason for this rather unsatisfactory state of affairs is that we do not yet have any direct observation of a star prior to its explosion as Type Ia supernova. We recently came a little closer to achieving this 'holy grail' of supernova research, with the early detection of SN 2011fe in the nearby galaxy M101. At a distance of 6.4 Mpc, this is the closest SN Ia in the past 25 years. As Figure 18.7 shows, no star is detected in the best pre-supernova images of this frequently observed large spiral galaxy. The non-detection improves very significantly previous empirical limits on the luminosity of the secondary (which were not very constraining; see Figure 18.8), although they are not sufficiently stringent to distinguish between single- and double-degenerate scenarios.

Thanks to regular and frequent sky monitoring, many recent supernovae

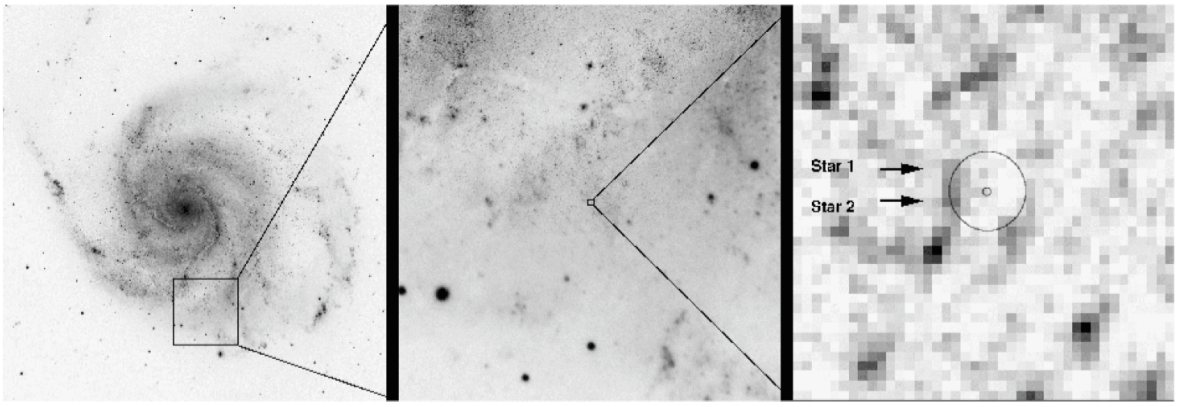

Figure 18.7: The recent bright ($V_{\rm max} = 10$) Type Ia supernova in the nearby ($d = 6.4$ Mpc) spiral galaxy M101 shows no obvious counterpart in archival *HST* images. The two concentric circles in the right-hand panel have radii corresponding to the 1σ (21 mas) and 9σ astrometric uncertainty in the position of the SN. (Figure reproduced from Li et al. 2011, arXiv:1109.1593).

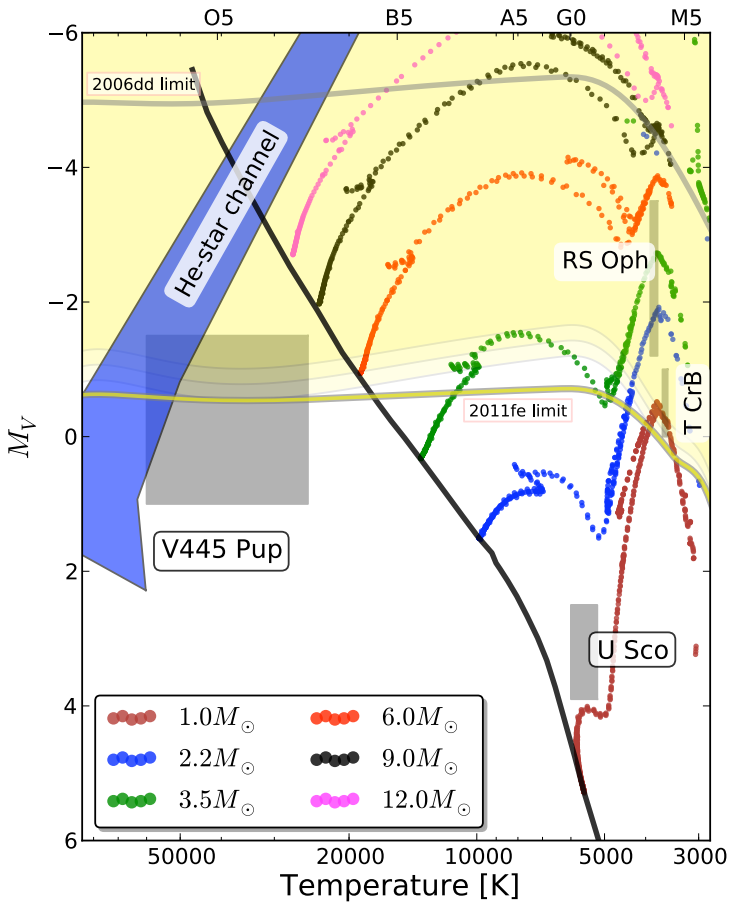

Figure 18.8: Progenitor system constraints for SN2011fe on the H-R diagram. The yellow area of the H-R diagram is excluded by the non-detection of a stellar counterpart at the position of SN2011fe in archival *HST* images of M101. The proximity of this galaxy has reduced significantly the allowed combination of effective temperature and luminosity of the progenitor, compared to the best previous limit, indicated by the grey line labelled '2006dd limit' near the top of the diagram. In the single-degenerate model, the secondary companion to the star that exploded as SN2011fe must have been of relatively low luminosity, either a red giant star evolved from $M_{\rm ZAMS} \lesssim 3.5 M_\odot$, or a main sequence star with $M \lesssim 5 M_\odot$. (Figure reproduced from Li et al. 2011, arXiv:1109.1593).

have been detected at very early times. It is estimated that the first photometry of SN2011fe was obtained only 11 hours after the explosion. At such early times, the luminosity can be related (with a few assumptions) to the initial radius of the star, R_0. From such considerations, Bloom et al. (2011, arXiv:1111.0966) were able to place the limit $R_0 \lesssim 0.02 R_\odot$, consistent with a white dwarf progenitor. Early spectral observations also showed high velocity (up to 20 000 km s^{-1}) C and O features, as well heavier elements synthesised in the explosion. The presence of C and O in the spectra favour the progenitor being a CO white dwarf.

Quoting from the recent review by Bo Wang (Research in Astronomy and Astrophysics, Vol.**18**, No.**5** 49, arXiv:1801.04031): *"The issue of the progenitors of SNe Ia is still poorly understood. There is still no single progenitor model that can reproduce all the observational features and full diversity of SNe Ia. So far, it seems that two or more progenitor models may contribute, although the fraction of SNe Ia from each model is really uncertain."*